Food Chemistry 160 (2014) 330–337

Contents lists available at ScienceDirect

Food Chemistry

journal homepage: www.elsevier.com/locate/foodchem

Combination of spectra and texture data of hyperspectral imaging for prediction of pH in salted meat

Dan Liu [a], Hongbin Pu [a], Da-Wen Sun [a,b,*], Lu Wang [a], Xin-An Zeng [a]

[a] College of Light Industry and Food Sciences, South China University of Technology, Guangzhou 510641, PR China
[b] Food Refrigeration and Computerised Food Technology, Agriculture and Food Science Centre, University College Dublin, National University of Ireland, Belfield, Dublin 4, Ireland

ARTICLE INFO

Article history:
Received 17 October 2013
Received in revised form 21 February 2014
Accepted 19 March 2014
Available online 27 March 2014

Keywords:
Hyperspectral imaging
Spectra
Texture
Porcine meat
pH
GLGCM

ABSTRACT

This study was carried out to investigate the feasibility of combining spectral with texture features in order to improve pH prediction for salted pork. Average spectra were extracted from the region of interest (ROI) of hyperspectral images over the wavelength region of 400–1000 nm and 9 characteristic spectral variables were then selected by principal components analysis (PCA). Meanwhile, gray-level gradient cooccurrence matrix (GLGCM) analysis was implemented on the first PC image (accounted for 96% of the total variance) to extract 13 textural feature variables. Partial least-squares regression (PLSR) was developed for predicting pH based on spectral, textural or combined data. Coefficient of determination (R^2_P) of 0.794 for the prediction samples based on data fusion was achieved, which was superior to the results based on spectra ($R^2_P = 0.783$) or texture ($R^2_P = 0.593$) alone. Hence, methods of combining spectral with texture analyses are effective for improving meat quality prediction.

1. Introduction

In the modern agri-food industry, quality is a key factor in determining the success of the industry. Therefore significant efforts have been made by the industry to enhance the quality of agricultural and food products that they produce by applying new technologies such as novel cooling (Sun, 1997; Sun, & Brosnan, 1999; Sun, & Zheng, 2006; Sun & Hu, 2003; Wang, & Sun, 2001; Hu, & Sun, 2000), freezing (Delgado, Zheng, & Sun, 2009; Zheng & Sun, 2006), drying (Sun, 1999; Sun, & Byrne, 1998; Sun, & Woods, 1993;1994a;1994b;1994c;1997; Cui, Xu, & Sun, 2004) and edible coating (Xu, Chen, & Sun 2001). In addition, great efforts have also been made to utilise emerging techniques for product quality evaluation and assurance. Among these techniques, also known as spectroscopic imaging, imaging spectroscopy or chemical imaging, is concerned with the combination of conventional digital imaging or computer vision (Du, & Sun, 2005; Jackman, Sun, Du, & Allen, 2008; Valous, Mendoza, Sun, & Allen, 2009) with spectroscopy to conduct measurement, analysis, and interpretation of both spatial and spectral information from a specific object simultaneously (Elmasry, Barbin, Sun, & Allen, 2012c; Goetz, Vane, Solomon, & Rock, 1985; Gowen, O'Donnell, Cullen, Downey, & Frias, 2007; Lorente, Aleixos, & Gomez-Sanchis, 2012; Sun, 2010; Van der Meer & De Jong, 2001). Although originally developed for remote sensing applications, HSI has recently found increasingly widespread use for quality and safety evaluation and control in the food industry with remarkable improvements in information and data processing techniques (Gowen, O'Donnell, Cullen, Downey, & Frias, 2007; Sun, 2010; Magwaza, Opara, Nieuwoudt, Cronje, Saeys, & Nicolaï, 2012). This technique is considered as non-time-consuming and non-destructive, with minimum human intervention. Consequently, HSI has become an attractive choice among different instrumental methods developed for the estimation of quality attributes in meat and meat products (Elmasry, Barbin, Sun, & Allen, 2012) including speedy evaluation of chemical (Barbin, Elmasry, Sun, & Allen, 2013; Talens et al., 2013), microbiological (Barbin, Elmasry, Sun, Allen, & Noha, 2012; Park et al., 2011) and quality attributes (Kamruzzaman, Elmasry, Sun, & Allen, 2013; Liu, Qu, Sun, Pu, & Zeng, 2013). Among many meat products (Chabbouh, Hadj Ahmed, Farhat, Sahli, & Bellagha, 2012; de Paula, Colet, de Oliveira, Valduga, & Treichel, 2011; Ferrentino, Balzan, & Spilimbergo, 2013; Sánchez-Zapata, Díaz-Vela, Pérez-Chabela, Pérez-Alvarez, & Fernández-López, 2013; Wesierska, Szołtysik, & Rak, 2013; Zell, Lyng, Morgan, & Cronin, 2013), salted meat is consumed in many countries due to its flavour and longer shelf life. It is known that salt added to the meat system can promote protein

* Corresponding author at: Food Refrigeration and Computerised Food Technology, Agriculture and Food Science Centre, University College Dublin, National University of Ireland, Belfield, Dublin 4, Ireland. Tel.: +353 1 7167342; fax: +353 1 7167493.
E-mail address: dawen.sun@ucd.ie (D.-W. Sun).
URLs: http://www.ucd.ie/refrig, http://www.ucd.ie/sun (D.-W. Sun).

http://dx.doi.org/10.1016/j.foodchem.2014.03.096
0308-8146/

extraction due to the high ionic forces in the media (Claus, Jhung-Won, & Flick, 1994). Protein precipitation and solubilization could induce a pH evolution in meat products throughout the salting process. Data of pH is closely related to the water holding capacity and water loss in salted and dry cured meat (Hamoen, Vollebregt, & Van der Sman, 2013). As an important meat quality indicator, meat pH varies with meat genetic origin, ante-mortem treatment, muscle and fibre type as well as manufacturing processes, such as salting temperature, salting periods and salting methods (Gou, Comaposada, & Arnau, 2002). Several studies have shown that pH is a good predictor of the colour and drip loss of meat. There is a high relationship between pH and moisture diffusivity and mechanical and sensory textural properties in salted or dry-cured meat (Gou et al., 2002; Guerrero, Gou, & Arnau, 1999; Ruiz-Ramirez, Arnau, Serra, & Gou, 2006). Therefore, the pH value is a fundamental datum to be monitored during the salting or marination process, because it gives a reasonably good indication of the final meat quality. Previous studies have revealed the possibility of employing HSI to predict the pH in meat and meat products (Qiao et al., 2007; Barbin, Elmasry, Sun, & Allen, 2012; Elmasry, Sun, & Allen, 2012; Iqbal, Sun, & Allen, 2013. Elmasry, Sun, and Allen (2012b) performed non-destructive HSI analysis of quality attributes of beef and obtained a coefficient of determination (R^2_{CV}) of 0.71 and root mean square errors of cross-validation (RMSECV) of 0.07 for predicting pH. Also Iqbal et al. (2013) develop a HSI system in the near infrared (NIR) region (900–1700 nm) to predict pH in cooked, pre-sliced turkey hams, and with the selected optimal wavelengths, a R^2_{CV} of 0.81 and RMSECV of 0.02 was achieved. Barbin et al. (2012) used the same system for pH prediction of fresh pork meat and a R^2_{CV} of 0.87 with RMSECV of 0.1 for pH prediction was obtained by partial least square (PLS) regression models. These studies reflected reasonable accuracy and robustness of pH prediction models based on hyperspectral data. However, most of these models were established based on spectral data without incorporating information on spatial data. The importance of analyzing spatial and spectral patterns simultaneously has been emphasized (Gupta, Chung, Srinath, Molfese, & Kook, 2005; Kotwal & Chaudhuri, 2013; Plaza et al., 2009; Pohl & Van Genderen, 1998; Polidori & Mangolini, 1996) and several authors (Huang, Zhao, Chen, & Zhang, 2013; Nanyam, Choudhary, Gupta, & Paliwal, 2012; Wang, Huang, & Zhu, 2012; Zhu, Zhang, He, Liu, & Sun, 2013) have attempted to explore the feasibility of data fusion to improve the performance of hyperspectral prediction models related to food analysis. Nanyam et al. (2012) developed a multi-band decision-fusion strategy for improving the performance of hyperspectral-imaging based fruit inspection systems. Decision-fusion techniques were employed to combine the decisions of selected univariate classifiers and as a result better classification was achieved for bruise detection in strawberries. Wang et al. (2012) also developed a fusion model using uninformative variable elimination (UVE)-PLS and supervised affinity propagation (SAP)-PLS models coupled with backpropagation neural network. A better prediction accuracy (R_P = 0.828 and RMSEP = 5.53 N) was achieved for apple firmness prediction. In addition, Zhu et al. (2013) used a visible and near infrared HSI system to differentiate between fresh and frozen–thawed fish based on combined spectral and textural variables by least squares-support vector machine classification models. An average correct classification rate of 97.22% for the prediction samples was achieved, which was superior to the results based on either spectral or textual information. Recently, the feature variables from spectral and image information of hyperspectral image datacube were also fused for rapid detection of total viable count (TVC) in pork meat (Huang et al., 2013). The back propagation artificial neural network (BP-ANN) model based on data fusion was better than models based on spectral or image variables, which was achieved with root mean square errors of prediction (RMSEP) of 0.243 lg CFU/g and coefficient of determination (R^2_P) of 0.8308 in the prediction set. This demonstrates that HSI combined with data fusion would be more useful for non-destructive analysis and predictions.

The main focus of the current research was to make a fusion of the spatial and spectral information space of the hypercube to improve pH prediction of pork in a salting process. It is known that the amount of information derived from the hyperspectral datacube requires the use of data fusion technique to take advantage of the complementarities that both sources of information can provide. Therefore, the specific objectives were to (1) extract spectral data from hyperspectral images of salted pork slices acquired in the NIR range (400–1000 nm); (2) identify the most significant spectral characteristic variables; (3) extract texture feature variables from characteristic images; (4) combine spectral with texture variables by feature level fusion, and (5) build new quantitative pH prediction models with spectra, textural and combined variables by PLSR.

2. Materials and methods

The main steps of the experimental procedure are presented in Fig. 1, which are mainly composed of image acquisition and preprocessing, spectral and textural extraction, feature integration and normalization and PLS analysis. Details of experimental procedures are introduced below.

2.1. Meat sample preparation

In this study, one hundred and fifty-two pork slices (7 mm) from the same anatomical locations (*longissimus dorsi*) of three pig carcasses were prepared manually, and meat slices were trimmed to nearly the size (90 mm × 60 mm × 7 mm) by a meat cutting knife. Visible fat and connective tissues were weeded out. Salting treatment was conducted by employing 30% NaCl (w/w) on the meat slices at room temperature of 25 °C for different salting stages (0, 15, 60, and 150 min). After salting treatment, visible fat and connective tissues were weeded out and surface moisture was wiped by paper towels before image acquisition. Prior to the analysis of the samples and model development, all samples were divided into two subsets, namely, calibration set consisting of 100 samples (25 samples × 4 periods) and validation set consisting of 52 samples (13 samples × 4 periods). Samples in the calibration set were used to establish the model, while samples in the prediction set were applied to verify the robustness of the established model. pH was measured randomly at four different locations across the sample surface with a pH meter (205-pH, Testo Instruments International Trading Co., Ltd., Shanghai, China). The average of the four pH readings was used to represent the ultimate pH value of the sample.

2.2. Hyperspectral imaging system and image processing

Prior to image acquisition, the hyperspectral imaging system was opened for preheating for 30 min. At the same time, meat slices were put onto the translation stage driven by a stepper motor (IRCP0076-1COMB, Isuzu Optics Corp., Taiwan, China) and go through the field of view (FOV) of the spectrograph (Imspector V10E, Spectral Imaging Ltd., Oulu, Finland) with an optimized speed of 1.5 mm s^{-1} the exposure time of CCD camera was set to 30 ms. Sample images were taken when the light provided by two tungsten-halogen lamps (3900-ER, Illumination Technologies Inc., New York, USA) were reflected from the meat surface, dispersed in a spectrograph, projected to a CCD camera (DL-604M, Andor, Ireland) and then transformed into a digital signal by image acquisition software (Spectral Image Software, Isuzu Optics Corp.,

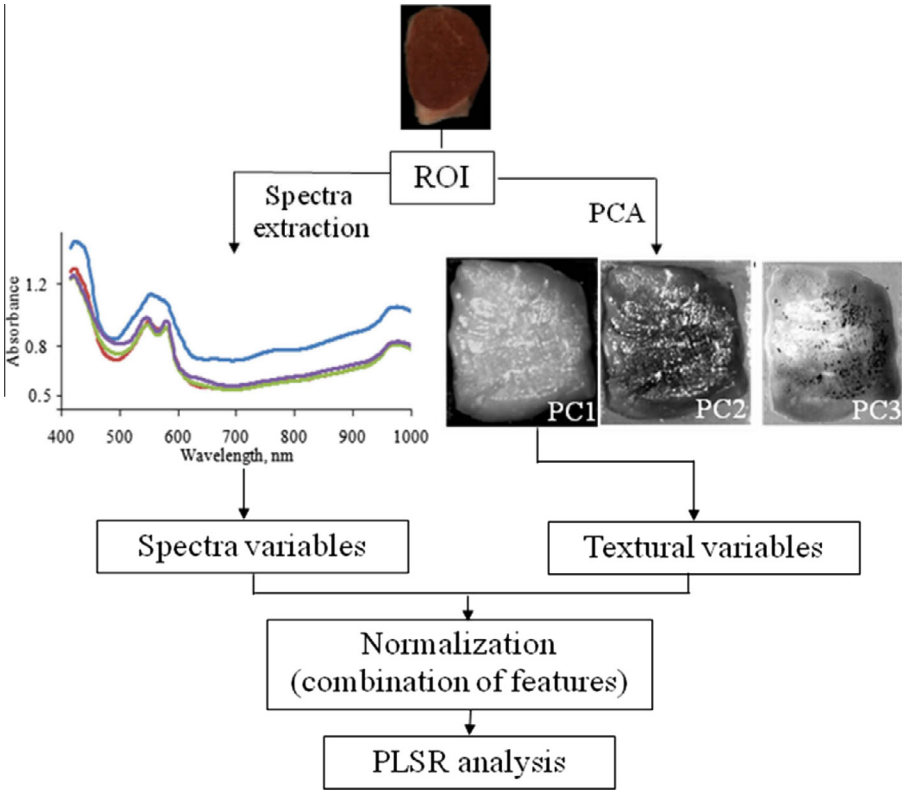

Fig. 1. Flowchart of main steps in data fusion analysis for predicting pH of meat product.

Taiwan, China) installed on a personal computer. The working spectral range of the system is 308–1105 nm with a spectral resolution of about 1.5 nm between the contiguous bands, thus producing a total of 501 bands. The system scans a single spatial line of the sample, and the reflected light was dispersed by the spectrograph in spatial–spectral axis. Once a sample entered the FOV, the hyperspectral data was captured and sent to the PC through a USB port for storage.

To correct dark current effect of the camera, each raw hyperspectral image was corrected by the following equation:

$$R_c = \frac{R_r - B}{W - B} \times 100\% \quad (1)$$

where R_c is the reflectance of corrected hyperspectral image, R_r is the reflectance of the raw hyperspectral image, B is the dark current image (~0% reflectance) acquired with the camera lens completely covered with its opaque cap, W is the white reference image (~99.9% reflectance) acquired for a standard Teflon calibration tile.

2.3. Spectral variables extraction

Due to the low signal-to-noise ratio at the starting and ending spectral region, only spectra within the range of 415–1000 nm were employed for spectral variable extraction. After image acquisition and calibration, the region of interests (ROIs) can be easily identified based on segmentation with a simple thresholding due to the distinctive spectral differences between meat sample and background spectrum. For each of the calibrated images, a mask was created by thresholding a gray image that was produced by subtracting the image at band 91 (of low reflectance value) from the image at band 255 (of high reflectance value). The resulted image was then segmented by a simple thresholding of 0.149, which was determined by creating a histogram. A region of interest (ROI) with a size of 300 × 200 pixels around the center of the image was selected for extracting reflectance spectra which was transformed into an absorbance profile by,

$$A = -\log_{10} R_c \quad (2)$$

where A is absorbance.

Principal component analysis (PCA) was used to select the optimum spectral variables. PCA is a common technique for dimension reduction and variable selection in multivariate data analysis (Liu, Zeng, & Sun, 2013a). In the processing of hyperspectral images, the spectral data matrix is decomposed by PCA into a product of a loading matrix, a score matrix and a residual matrix (Jolliffe, 2002). The scores of PCA represent the weighted sums of the original variables, and the loadings of PCA are the weighting coefficients for each variable (wavelength) at each principal component and can be used to identify important variables (wavelengths). In this way, wavelength selection contributes in reducing the number of spectral variables which are irrelevant and have minor impact on data variation. Background segmentation and extraction of reflectance spectra from the hyperspectral images was carried out using the software ENVI 4.8 (ITT Visual Information Solutions, Boulder, CO, USA). PCA was performed with the aid of chemometric software (Unscrambler version 9.7, CAMO, Trondheim, Norway).

2.4. Textual variables extraction

Gray-level-gradient co-occurrence matrix analysis (GLGCM) is a texture analysis technique, which captures the second order statistics of gray level gradients. GLGCM characterizes typically the spatial relationships of two basic elements of an image: gray and gradient and can depict effectively texture characteristics by the change of the gradient of gray levels (Hong, 1984). GLGCM was implemented on the first PC score image to extract textural feature variables. A total of 13 s-order statistical textural variables

(energy, correlation, hybrid entropy, inertia, gray mean, grads mean, gray entropy, grads entropy, gray standard deviation, grads standard deviation, inverse difference moment, small grads dominance, and big grads dominance) were extracted from the first PC image in this study. The calculation of textural variables for all ROI images of all samples produced a textural matrix of 152 samples × 13 variables. The GLGCM parameters were calculated using a program written in Matlab (Version 9, The Mathworks Inc., Massachusetts, USA).

2.5. Features integration

Data fusion aims at combining disparate with complementary data from multisource imagery to obtain more information from the images as well as to improve reliability of operational performance. Generally, data fusion can be performed at three different processing levels: pixel level fusion, feature level fusion and decision level fusion (Pohl & Van Genderen, 1998). Pixel level fusion is the direct merging of the original data in various data sources and requires immense data calculation; fusion at feature level requires the extraction of feature variables and then fuses for further assessment using statistical approaches such as arithmetic combinations, filters, regression variable substitution and wavelets in a multi resolution image; and decision level fusion is based on a pre-knowledge of the observed object and combining the extracted information by applying decision rules to achieve the required results (Huang et al., 2013; Pohl & Van Genderen, 1998). To avoid the huge data preprocessing and potential information losses, the feature variables from spectral and image information of hypercube were fused by feature level fusion for further analysis.

Another relevant issue in order to make full use of the benefits of data fusion is to overcome the problem of the large disparity in values among the feature parameters (Mendoza, Lu, Ariana, Cen, & Bailey, 2011). A potential problem during the data fusion procedure is that a large-value parameter would hide the predicting power of smaller value parameter(s), which may be as important as, or even more important than large-value parameter(s). In the current study, a classical mean normalization procedure was applied to rescale the difference in values of the absorbance spectra and texture feature as follows:

$$Y_{N,i} = Y_i/\overline{Y} \quad (3)$$

where $Y_{N,i}$ denotes the normalized parameter for sample i, Y_i is the original parameter for sample i and $\overline{Y}$ is the mean value. This normalization procedure was applied to both calibration and validation sets and resulted in a similar scale of values. Partial least squares (PLS) method was then applied to develop pH calibration models using the integrated features.

2.6. PLS prediction model

PLS regression is a popular chemometric method for building calibration models, which suit constructing empirical predictive models when the experimental factors are numerous and highly collinear (Wold, Sjostrom, & Eriksson, 2001). The quantitative models between pH and feature data extracted from porcine meat at different salting periods were established using partial least squares regression (PLSR). The feature data utilized here included four categories, i.e., full-wavelength spectra and simplified spectra selected by PCA; textural variables calculated by GLGCM and fused features. Therefore, four categories of PLSR calibration models were built. The quality of calibration models were evaluated by root mean squared errors for calibration, cross-validation as well as prediction (RMSEC, RMSECV and RMSEP, respectively), and coefficients of determination for calibration, cross-validation and prediction (R^2_c, R^2_{CV} and R^2_P, respectively). All computations and multivariate data analysis was performed by Unscrambler chemometric software (Version 9.7, CAMO, Trondheim, Norway).

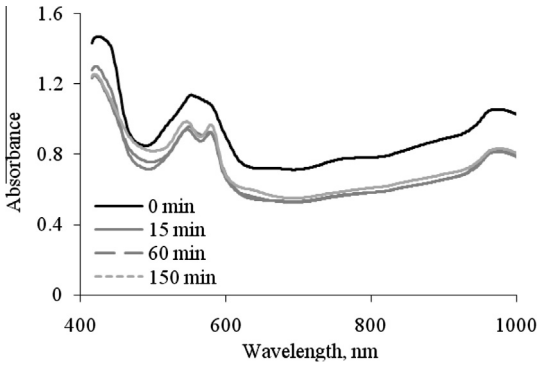

Fig. 2. The mean absorbance curves for salted meat in wavelength range of 400–1000 nm.

3. Results and discussion

3.1. Spectral features of salted meat

Fig. 2 shows mean VIS/NIR absorbance curves in the range of 400–1000 nm for pork meat collected during the salting stages. The general trends of the spectral curves were similar. It was also noticed that the fresh meat (salted 0 min) differed to a large extent from the other three salted samples in the magnitude of absorbance possibly due to the water loss during salting process. The absorbance on the wavebands from 540 to 580 nm is associated with respiratory pigment (Qiao et al., 2007). The absorption bands due to the presence of water in the meat could be clearly observed at 750 and 970 nm, which arose from combination of symmetric and antisymmetric O–H stretching and bending modes (Liu et al., 2013). More specifically, during the salting of meats, salt diffusion caused tissue damage and texture alteration, as well as the disruption and leakage of various cellular organelles. The existence of these differences and changes suggested that it might be possible to predict pH by spectroscopic and textural analysis of hyperspectral images.

3.2. Selection of optimum characteristic image and optimal spectral variables by PCA

Texture features exhibited in hyperspectral images vary with both spectral and spatial parameters, so the selection of gray level images is important to obtain good prediction accuracy. PCA was first carried out for all ROI images to reduce spectral dimension, with several principal components (PCs) accounting for the most variances of all spectral bands. Fig. 3a shows the score plots of the first two PCs from PCA conducted on the full spectral data of salted meats. It was found that the majority of the variance was captured by the first three PCs, as shown in the score plot, where PC1, PC2, and PC3 explained 96%, 2% and 1% of variance, respectively. Thus, the first principal component (PC1) image could be used as the best representation of the original sample and was selected for the textural information extraction in each ROI image, leading to 13 textural variables (Table 1) being extracted by GLGCM from the PC1 score image. Also, a plot of variances with respect to the number of PC was presented in Fig 3b. The variance of the first three PCs could explain more than 95% of the total variance. So it was not necessary for the consideration of more than three PCs.

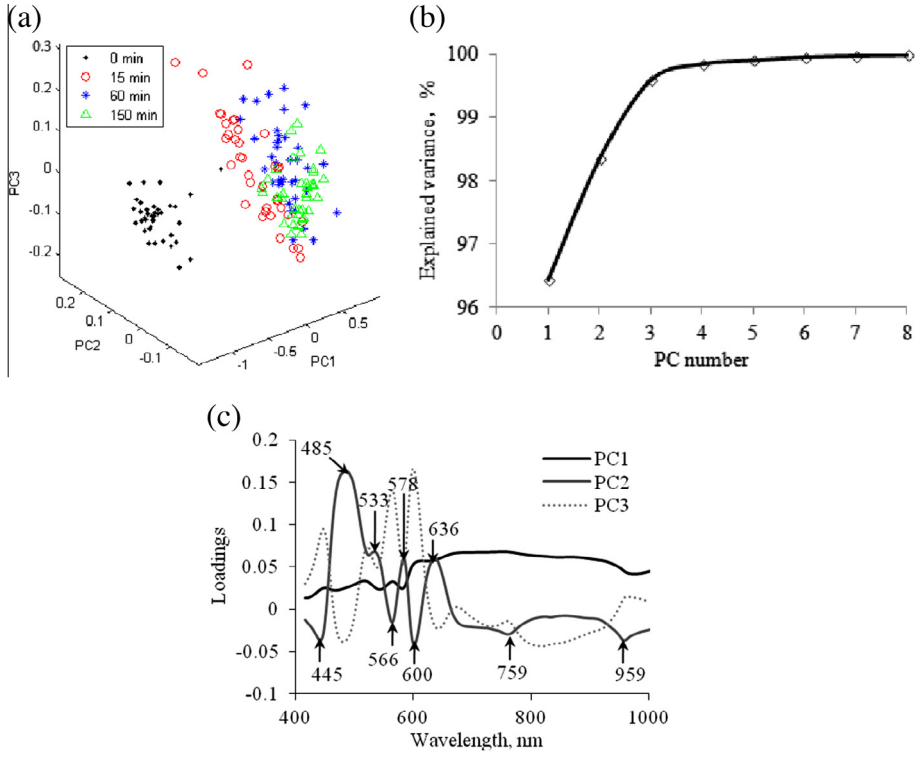

Fig. 3. (a) Representation of the score plots of PCA. (b) Plot of variances with respect to the number of PC. (c) Loadings of the first three PCs showing the selected wavelengths.

Table 1
Texture features extracted from GLGCM matrix.

Feature	Equation
Small grads dominance	$T_1 = \left[\sum_{i=1}^{n}\sum_{j=1}^{n}\frac{H(i,j)}{j^2}\right] \Big/ \left[\sum_{i=1}^{n}\sum_{j=1}^{n}H(i,j)\right]$
Big grads dominance	$T_2 = \left[\sum_{i=1}^{n}\sum_{j=1}^{n}j^2H(i,j)\right] \Big/ \left[\sum_{i=1}^{n}\sum_{j=1}^{n}H(i,j)\right]$
Energy	$T_3 = \sum_{i=1}^{n}\sum_{j=1}^{n}[P(i,j)]^2$
Inertia	$T_4 = \sum_{i=1}^{n}\sum_{j=1}^{n}(i-j)^2 \cdot P(i,j)$
Gray entropy	$T_5 = -\left\{\sum_{i=1}^{n}\left[\sum_{j=1}^{n}P(i,j)\right] \cdot \log\left[\sum_{j=1}^{n}P(i,j)\right]\right\}$
Grads entropy	$T_6 = -\left\{\sum_{j=1}^{n}\left[\sum_{i=1}^{n}P(i,j)\right] \cdot \log\left[\sum_{i=1}^{n}P(i,j)\right]\right\}$
Hybrid entropy	$T_7 = -\sum_{i=1}^{n}\sum_{j=1}^{n}P(i,j) \cdot \log P(i,j)$
Gray mean	$\mu_1 = \sum_{i=1}^{n} i \cdot \left[\sum_{j=1}^{n}P(i,j)\right]$
Grads mean	$\mu_2 = \sum_{j=1}^{n} j \cdot \left[\sum_{i=1}^{n}P(i,j)\right]$
Gray standard deviation	$\partial_1 = \left\{\sum_{i=1}^{n}(i-\mu_1)^2\left[\sum_{j=1}^{n}P(i,j)\right]\right\}^{1/2}$
Grads standard deviation	$\partial_2 = \left\{\sum_{j=1}^{n}(i-\mu_2)^2\left[\sum_{i=1}^{n}P(i,j)\right]\right\}^{1/2}$
Correlation	$T_8 = \frac{1}{\partial_1\partial_2}\sum_{i=1}^{n}\sum_{j=1}^{n}(i-\mu_1)(j-\mu_2)P(i,j)$
Inverse difference moment	$T_9 = \sum_{i=1}^{n}\sum_{j=1}^{n}\frac{1}{1+(i-j)^2}P(i,j)$

The loadings resulting from PCA could be used to identify optimal variables (wavelengths) that were responsible for the specific features appeared in the corresponding scores. The loadings of PC1, PC2 and PC3 were used for wavelength selection as shown in Fig. 3c. The wavelengths corresponding to peaks and valleys at these particular principal components were selected as optimum wavelengths. PC1 explained 96% of the total variance in the samples but the loadings of the first PC had small variances, thus no wavelength was selected from this component. On the other hand, the maxima and minima of the loadings from the second and third PCs were opposite, resulting in the selection of a total of nine important wavelengths (445, 485, 533, 566, 578, 600, 636, 759 and 959 nm). The nine selected optimal wavelengths had minimal redundancy and were used for predicting the pH values of salted pork samples.

3.3. Prediction of pH using PLSR models

The prediction of meat pH value was performed by using PLSR, in which an independent variable pH was predicted from full spectral variables (371 wavelengths), optimal spectral variables (9 wavelengths), textural variables (13 textures) and combined feature variables (9 wavelengths and 13 textures). Table 2 shows the main statistics used to evaluate the performance of the developed calibration, cross-validation and prediction models for predicting pH of the examined pork samples. To visualize graphically the performance of the PLSR models, the measured values obtained from the laboratory measurements and its predicted values resulting from the four established PLSR models in prediction set are plotted and displayed in Fig. 4. The PLSR model based on full spectra exhibited a good capability to predict pH with the highest correlation coefficients of 0.856, 0.847 and 0.797 as well as the lowest RMSEs of 0.074, 0.077 and 0.085 for calibration cross-validation and prediction, respectively (Table 2). Although the pH cannot be measured directly by the HSI system as in the case with H+ sensitive electrodes, the analysis can be realized by registering the differences in absorbance patterns due to the probably increased solubility of meat compounds such as free amino acids, peptides, proteins, minerals, lactate and lactic acid with increasing salting

Table 2
Performance of PLSR (full and simplified) for the prediction pH of salted meat with different characteristic information.

Model	No. of variable	LV	Calibration		Cross-validation		Prediction	
			R^2_c	RMSEC	R^2_{CV}	RMSECV	R^2_P	RMSEP
Model based on full spectra	371	3	0.856	0.074	0.847	0.077	0.797	0.085
Model based on optimal spectra	9	7	0.842	0.0776	0.834	0.0804	0.783	0.088
Model based on textures	13	6	0.643	0.1166	0.625	0.1207	0.593	0.1209
Model based on data fusion	384	4	0.855	0.074	0.845	0.078	0.796	0.085
	22	6	0.853	0.0748	0.841	0.0786	0.794	0.086

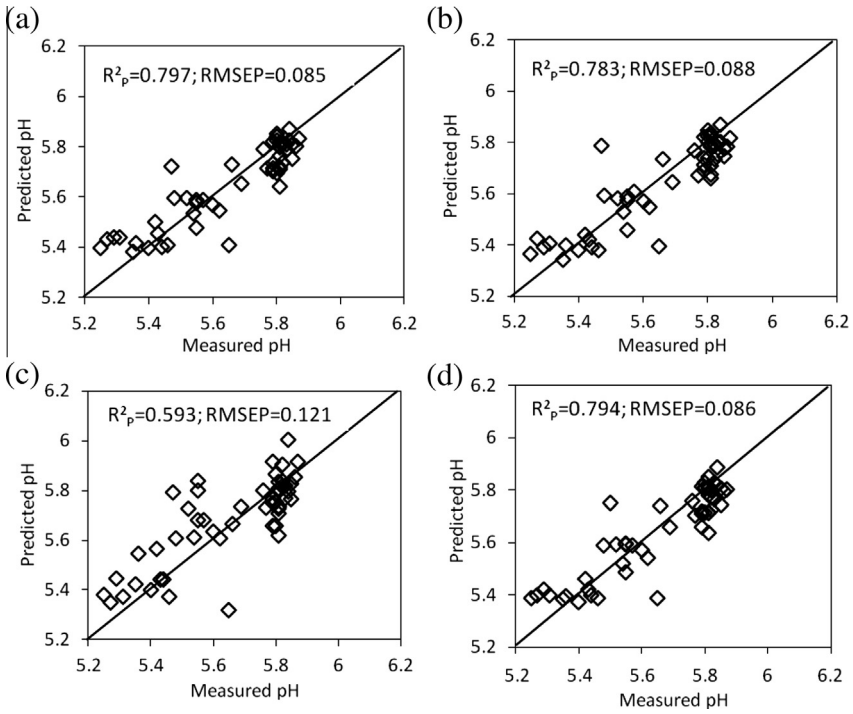

Fig. 4. Measured and predicted pH values for validation sets by PLS methods using four models. (a) model based on full spectra; (b) model based on optimal spectra; (c) model based on image; (d) model based on data fusion.

time (Goli, Bohuon, Ricci, & Collignan, 2012). Consequently, a change of pH levels in the meat might be expected during salting process. Although the accuracy of PLSR model based on optimal spectra was slightly reduced in pH prediction (Fig. 4b), the implementation of a fewer number of wavelength variables could reduce the time required for image acquisition, for example the total acquisition time of about 3.5 s can reduce to only 0.09s if the acquired bands number change from 371 bands to 9 bands. Thereby improving data acquisition and processing speed. Compared to models based on spectral data, the model based on image information has a lower prediction performance with the correlation coefficients of 0.593 and RMSEP of 0.121 (Fig. 4c). This might be because the spectral data had greater contribution than the textural features in building the PLSR model. Spectral information can explain the internal attributes (chemical compositions, tissue structure, etc.) in pork meat, which are closely related to pH changes, while textural changes occurred during the salting process do not have significant correlation with the pH evolution, hence, the prediction result is not very satisfying (see Fig. 4c). As for the model based on data fusion, which combined both the external and internal attributes in pork meat, it could explain more fully the pH change in pork meat, leading to better prediction results (see Fig. 4d). The predictability of pH obtained by data fusion in this study was higher than those obtained by Qiao et al. (2007) using pork with $r_p = 0.55$ and RMSEP = 0.21; by Elmasry et al. (2012b) using beef with $R^2_{CV} = 0.71$ and RMSECV = 0.07 and by Iqbal et al. (2013) for cooked, pre-sliced turkey hams with $R^2_{CV} = 0.81$ and RMSECV = 0.02. However, the performance of the developed pH prediction model was inferior to that obtained by Barbin, Elmasry, Sun, and Allen (2012a) for pork with $R^2_{CV} = 0.87$ and RMSECV = 0.1. These differences could be due to the different spectral range, sample origin and feature extraction methods with respect to pH prediction. Although the improvement by integration of spectral with textural features was limited, it is still interesting and encouraging for further research to investigate the correlation of other meat quality and fused feature extracted from hyperspectral images.

4. Conclusions

Salting is the stage to be controlled and modified to obtain a final product of the appropriate quality. In this research, spectral and image information from hyperspectral datacube was combined for determining pH of porcine meat during the salting process. Results showed that the combination of spectra and texture features was more effective than when the spectra or texture features were used alone for evaluating meat pH. A R^2_P of 0.794 and RMSEP of 0.086 were obtained based on combined feature of spectra with texture. However, pH prediction with texture variables selected by GMGLC was poor with R^2_P of 0.593. More efforts should be directed on advanced textural feature extraction methods such as run length

matrix, multi-resolution wavelet transform and directional fractal dimension analysis. Additional work to identify the nature of the meat compounds solubilised during the salting process and the development of more appropriate data fusion methods for establishing robust prediction models would constitute a step towards an accurate pH prediction.

Acknowledgements

The authors are grateful to the Guangdong Province Government (China) for support through the program of "Leading Talent of Guangdong Province (Da-Wen Sun)". This research was also supported by Postdoctoral Science Foundation of China (2013M530366) and Fundamental Research Funds for the Central Universities of China (2014ZM0027).

References

Barbin, D. F., Elmasry, G., Sun, D.-W., & Allen, P. (2012a). Predicting quality and sensory attributes of pork using near-infrared hyperspectral imaging. *Analytica Chimica Acta, 719*, 30–42.

Barbin, D. F., Elmasry, G., Sun, D.-W., & Allen, P. (2013). Non-destructive determination of chemical composition in intact and minced pork by near-infrared hyperspectral imaging. *Food Chemistry, 138*, 1162–1171.

Barbin, D. F., Elmasry, G., Sun, D.-W., Allen, P., & Noha, M. (2012b). Non-destructive assessment of microbial contamination in porcine meat using NIR hyperspectral imaging. *Innovative Food Science & Emerging Technologies, 17*, 180–191.

Chabbouh, M., Hadj Ahmed, S. B., Farhat, A., Sahli, A., & Bellagha, S. (2012). Studies on the Salting Step of Tunisian Kaddid Meat: Experimental Kinetics, Modeling and Quality. *Food and Bioprocess Technology, 5*(5), 1882–1895.

Claus, J. R., Jhung-Won, C., & Flick, G. J. (1994). Processed meats/poultry/seafood. In D. M. Kinsman, A. W. Kotula, & B. C. Breidenstein (Eds.), *Muscle foods: Meat, poultry, and seafood technology*. New York: Chapman and Hall.

Cui, Z. W., Xu, S. Y., & Sun, D.-W. (2004). Effect of microwave-vacuum drying on the carotenoids retention of carrot slices and chlorophyll retention of chinese chive leaves. *Drying Technology, 22*(3), 563–575. http://dx.doi.org/10.1081/DRT-120030001.

Delgado, A. E., Zheng, L. Y., & Sun, D.-W. (2009). Influence of Ultrasound on Freezing Rate of Immersion-frozen Apples. *Food And Bioprocess Technology, 2*(3), 263–270.

de Paula, R., Colet, R., de Oliveira, D., Valduga, E., & Treichel, H. (2011). Assessment of Different Packaging Structures in the Stability of Frozen Fresh Brazilian Toscana Sausage. *Food and Bioprocess Technology, 4*(3), 481–485.

Du, C. J., & Sun, D.-W. (2005). Comparison of three methods for classification of pizza topping using different colour space transformations. *Journal of Food Engineering, 68*(3), 277–287.

Elmasry, G., Barbin, D. F., Sun, D.-W., & Allen, P. (2012a). Meat quality evaluation by hyperspectral imaging technique: An overview. *Critical Reviews on Food Science and Nutrition, 52*, 689–711.

Elmasry, G., Barbin, D. F., Sun, D.-W., & Allen, P. (2012c). Meat Quality evaluation by hyperspectral imaging technique: An overview. *Critical Reviews in Food Science and Nutrition, 52*(8), 689–711.

Elmasry, G., Sun, D.-W., & Allen, P. (2012b). Near-infrared hyperspectral imaging for predicting colour, pH and tenderness of fresh beef. *Journal of Food Engineering, 110*, 127–140.

Ferrentino, G., Balzan, S., & Spilimbergo, S. (2013). Supercritical Carbon Dioxide Processing of Dry Cured Ham Spiked with Listeria monocytogenes: Inactivation Kinetics, Color, and Sensory Evaluations. *Food and Bioprocess Technology, 6*(5), 1164–1174.

Goetz, A. F. H., Vane, G., Solomon, J. E., & Rock, B. N. (1985). Imaging spectrometry for Earth remote sensing. *Science, 228*, 1147–1153.

Goli, T., Bohuon, P., Ricci, J., & Collignan, A. (2012). Evolution of pH during immersion of meat protein matrices in acidic marinades. *Meat Science, 90*, 618–623.

Gou, P., Comaposada, J., & Arnau, J. (2002). Meat pH and meat fibre direction effects on moisture diffusivity in salted ham muscles dried at 5 °C. *Meat Science, 61*, 25–31.

Gowen, A. A., O'Donnell, C. P., Cullen, P. J., Downey, G., & Frias, J. M. (2007). Hyperspectral imaging-an emerging process analytical tool for food quality and safety control. *Trends in Food Science and Technology, 18*, 590–598.

Guerrero, L., Gou, P., & Arnau, J. (1999). The influence of meat pH on mechanical and sensory textural properties of dry-cured ham. *Meat Science, 52*, 267–273.

Gupta, L., Chung, B., Srinath, M. D., Molfese, D. L., & Kook, H. (2005). Multi-channel fusion models for the parametric classification of differential brain activity. *IEEE Transactions on Biomedical Engineering, 52*(11), 1869–1881.

Hamoen, J. R., Vollebregt, H. M., & Van der Sman, R. G. M. (2013). Prediction of the time evolution of pH in meat. *Food Chemistry, 141*, 2363–2372.

Hong, J. G. (1984). Gray level-gradient co-occurrence texture analysis method. *Acta Automatica Sinica, 10*, 22–25.

Hu, Z. H., & Sun, D.-W. (2000). CFD simulation of heat and moisture transfer for predicting cooling rate and weight loss of cooked ham during air-blast chilling process. *Journal of Food Engineering, 46*(3), 189–197.

Huang, L., Zhao, J., Chen, Q., & Zhang, Y. (2013). Rapid detection of total viable count (TVC) in pork meat by hyperspectral imaging. *Food Research International, 54*, 821–828.

Iqbal, A., Sun, D.-W., & Allen, P. (2013). Prediction of moisture, color and pH in cooked, pre-sliced turkey hams by NIR hyperspectral imaging system. *Journal of Food Engineering, 117*, 42–51.

Jackman, P., Sun, D.-W., Du, C.-J., & Allen, P. (2008). Prediction of beef eating quality from colour, marbling and wavelet texture features. *Meat Science, 80*(4), 1273–1281.

Jolliffe, I. T. (2002). *Principal component analysis* (2nd ed.). New York: Springer-Verlag.

Kamruzzaman, M., Elmasry, G., Sun, D.-W., & Allen, P. (2013). Non-destructive assessment of instrumental and sensory tenderness of lamb meat using NIR hyperspectral imaging. *Food Chemistry, 141*, 389–396.

Kotwal, K., & Chaudhuri, S. (2013). A novel approach to quantitative evaluation of hyperspectral image fusion techniques. *Information Fusion, 14*(1), 5–18.

Liu, D., Qu, J., Sun, D.-W., Pu, H., & Zeng, X.-A. (2013). Non-destructive prediction of salt contents and water activity of porcine meat slices by hyperspectral imaging in a salting process. *Innovative Food Science & Emerging Technologies*. http://dx.doi.org/10.1016/j.ifset.2013.09.002.

Liu, D., Zeng, X. A., & Sun, D.-W. (2013a). Recent Advances in Wavelength Selection Techniques for Hyperspectral Image Processing in the Food Industry. *Food and Bioprocess Technology*. http://dx.doi.org/10.1007/s11947-013-1193-6.

Lorente, D., Aleixos, N., & Gomez-Sanchis, J. (2012). Recent advances and applications of hyperspectral imaging for fruit and vegetable quality assessment. *Food and Bioprocess Technology, 5*, 1121–1142.

Magwaza, L. S., Opara, U. L., Nieuwoudt, H., Cronje, P. J. R., Saeys, W., & Nicolaï,, B. (2012). NIR Spectroscopy Applications for Internal and External Quality Analysis of Citrus Fruit-A Review. *Food and Bioprocess Technology, 5*(2), 425–444.

Mendoza, F., Lu, R., Ariana, D., Cen, H., & Bailey, B. (2011). Integrated spectral and image analysis of hyperspectral scattering data for prediction of apple fruit firmness and soluble solids content. *Postharvest Biology and Technology, 62*, 149–160.

Nanyam, Y., Choudhary, R., Gupta, L., & Paliwal, J. (2012). A decision-fusion strategy for fruit quality inspection using hyperspectral imaging. *Biosystems Engineering, 112*, 118–125.

Park, B., Yoon, S.-C., Windham, W., Lawrence, K., Kim, M., & Chao, K. (2011). Line-scan hyperspectral imaging for real-time in-line poultry fecal detection. *Sensing and Instrumentation for Food Quality and Safety, 5*, 25–32.

Plaza, A., Benediktsson, J. A., Boardman, J. W., Brazile, J., Bruzzone, L., Camps-Valls, G., et al. (2009). Recent advances in techniques for hyperspectral image processing. *Remote Sensing of Environment, 113*, S110–S122.

Pohl, C., & Van Genderen, J. L. (1998). Review article Multisensor image fusion in remote sensing: Concepts, methods and applications. *International Journal of Remote Sensing, 19*, 823–854.

Polidori, L., & Mangolini, M. (1996). Potentials and limitations of multisensor data fusion. Fusion of earth data - Proceedings EARSeL conference (pp. 13–19). Cannes, France (6–8 February).

Qiao, J., Wang, N., Ngadi, M. O., Gunenc, A., Monroy, M., Gariepy, C., et al. (2007). Prediction of drip-loss, pH, and color for pork using a hyperspectral imaging technique. *Meat Science, 76*, 1–8.

Ruiz-Ramirez, J., Arnau, J., Serra, X., & Gou, P. (2006). Effect of pH24, NaCl content and proteolysis index on the relationship between water content and texture parameters in *biceps femoris* and *semimembranosus* muscles in dry-cured ham. *Meat Science, 72*, 185–194.

Sánchez-Zapata, E., Díaz-Vela, J., Pérez-Chabela, M. L., Pérez-Alvarez, J. A., & Fernández-López, J. (2013). Evaluation of the Effect of Tiger Nut Fibre as a Carrier of Unsaturated Fatty Acids Rich Oil on the Quality of Dry-Cured Sausages. *Food and Bioprocess Technology, 6*(5), 1181–1190.

Sun, D.-W. (1997). Thermodynamic design data and optimum design maps for absorption refrigeration systems. *Applied Thermal Engineering, 17*(3), 211–221.

Sun, D.-W. (1999). Comparison and selection of EMC ERH isotherm equations for rice. *Journal of Stored Products Research, 35*(3), 249–264.

Sun, D.-W. (2010). *Hyperspectral imaging for food quality analysis and control*. Elsevier, San Diego, CA: Academic Press.

Sun, D.-W., & Brosnan, T. (1999). Extension of the vase life of cut daffodil flowers by rapid vacuum cooling. *International Journal of Refrigeration-Revue Internationale Du Froid, 22*(6), 472–478. http://dx.doi.org/10.1016/S0140-7007(99)00011-0.

Sun, D.-W., & Byrne, C. (1998). Selection of EMC/ERH isotherm equations for rapeseed. *Journal of Agricultural Engineering Research, 69*(4), 307–315.

Sun, D.-W., & Hu, Z. H. (2003). CFD simulation of coupled heat and mass transfer through porous foods during vacuum cooling process. *International Journal of Refrigeration-Revue Internationale Du Froid, 26*(1), 19–27. http://dx.doi.org/10.1016/S0140-7007(02)00038-5.

Sun, D.-W., & Woods, J. L. (1993). The moisture-content relative-humidity equilibrium relationship of wheat - a review. *Drying Technology, 11*(7), 1523–1551. http://dx.doi.org/10.1080/07373939308916918.

Sun, D.-W., & Woods, J. L. (1994a). Low-temperature moisture transfer characteristics of wheat in thin-layers. *Transactions of The Asae, 37*(6), 1919–1926.

Sun, D.-W., & Woods, J. L. (1994b). The selection of sorption isotherm equations for wheat-based on the fitting of available data. *Journal of Stored Products Research, 30*(1), 27–43.

Sun, D.-W., & Woods, J. L. (1994c). Low-temperature moisture transfer characteristics of barley - thin-layer models and equilibrium isotherms. *Journal of Agricultural Engineering Research, 59*(4), 273–283.

Sun, D.-W., & Woods, J. L. (1997). Simulation of the heat and moisture transfer process during drying in deep grain beds. *Drying Technology, 15*(10), 2479–2508.

Sun, D.-W., & Zheng, L. Y. (2006). Vacuum cooling technology for the agri-food industry: Past, present and future. *Journal of Food Engineering, 77*(2), 203–214. http://dx.doi.org/10.1016/j.jfoodeng.2005.06.023.

Talens, P., Mora, L., Morsy, N., Barbin, D. F., Elmasry, G., & Sun, D.-W. (2013). Prediction of water and protein contents and quality classification of Spanish cooked ham using NIR hyperspectral imaging. *Journal of Food Engineering, 117*, 272–280.

Valous, N. A., Mendoza, F., Sun, D.-W., & Allen, P. (2009). Colour calibration of a laboratory computer vision system for quality evaluation of pre-sliced hams. *Meat Science, 81*(1), 132–141.

Van der Meer, F. D., & De Jong, S. M. (2001). *Imaging spectrometry – Basic principles and prospective applications*. Macsource Press.

Wang, S., Huang, M., & Zhu, Q. (2012). Model fusion for prediction of apple firmness using hyperspectral scattering image. *Computers and Electronics in Agriculture, 80*, 1–7.

Wang, L. J., & Sun, D.-W. (2001). Rapid cooling of porous and moisture foods by using vacuum cooling technology. *Trends In Food Science & Technology, 12*(5–6), 174–184. http://dx.doi.org/10.1016/S0924-2244(01)00077-2.

Wesierska, E., Szołtysik, M., & Rak, L. (2013). Physico-chemical, Biochemical and Microbiological Properties of Traditional Polish Pork Fermented Products During Ripening. *Food and Bioprocess Technology, 6*(11), 2986–2995.

Wold, S., Sjostrom, M., & Eriksson, L. (2001). PLS-regression: A basic tool of chemometrics. *Chemometrics and Intelligent Laboratory Systems, 58*, 109–130.

Xu, S. Y., Chen, X. F., & Sun, D.-W. (2001). Preservation of kiwifruit coated with an edible film at ambient temperature. *Journal of Food Engineering, 50*(4), 211–216. http://dx.doi.org/10.1016/S0260-8774(01)00022-X.

Zell, M., Lyng, J. G., Morgan, D. J., & Cronin, D. A. (2012). Quality Evaluation of an Ohmically Cooked Ham Product. *Food and Bioprocess Technology, 5*(1), 265–272.

Zheng, L. Y., & Sun, D.-W. (2006). Innovative Applications of Power Ultrasound during Food Freezing Processes - A Review. *Trends in Food Science & Technology, 17*(1), 16–23.

Zhu, F., Zhang, D., He, Y., Liu, F., & Sun, D.-W. (2013). Application of visible and near infrared hyperspectral imaging to differentiate between fresh and frozen–thawed fish fillets. *Food and Bioprocess Technology, 6*, 2931–2937.